

# Design, Control, and Psychophysics of Tasbi: A Force-Controlled Multimodal Haptic Bracelet

Evan Pezent<sup>1</sup>, Member, IEEE, Priyanshu Agarwal<sup>1</sup>, Member, IEEE, Jessica Hartcher-O'Brien, Member, IEEE, Nicholas Colonnese, Member, IEEE, and Marcia K. O'Malley<sup>1</sup>, Fellow, IEEE

**Abstract**—Haptic feedback is known to enhance the realism of an individual's interactions with objects in virtual environments. Wearable haptic devices, such as vibrotactile sleeves or armbands, can provide haptic feedback in a smaller and more lightweight form factor than haptic gloves that can be bulky and cumbersome to the wearer. In this article, we present tactile and squeeze bracelet interface (Tasbi), a multimodal haptic wristband that can provide radial squeeze forces around the wrist along with vibrotactile feedback at six discrete locations around the band. Tasbi implements a squeezing mechanism that minimizes tangential forces between the band's points of contact with the skin, instead of focusing the motor actuation to predominantly normal forces. Force sensing capacitors enable closed-loop control of the squeeze force, while vibration is achieved with linear resonant actuators. A detailed description of the design and experimental results demonstrating closed-loop control of squeeze cues provided by Tasbi is presented. Additionally, we present the results of psychophysical experiments that quantify user perception of the vibration and squeeze cues, including vibrotactile identification accuracy in the presence of varying squeeze forces, discrimination thresholds for the squeeze force, and an analysis of user preferences for squeeze actuation magnitudes.

**Index Terms**—Bracelet, force control, multimodal, squeeze, vibration, wearable, wrist.

## I. INTRODUCTION

HAPTIC feedback, or technology that recreates the sense of touch, is a major field of research spanning the disciplines of robotics and human perception. Haptic devices have been extensively studied for the purpose of enhancing realism in virtual environments [1], closing the action-confirmation loop in user interfaces [2], improving the efficacy of training programs [3], and providing feedback to augment or substitute for other senses [4]. Guided by this promise, decades of research

and development have given rise to numerous haptic technologies ranging from simple one degree-of-freedom actuators that vibrate the skin, to electrostatic surfaces that render texture on the finger, to highly articulated robotic manipulators and exoskeletons that transmit kinesthetic forces to the hands or limbs. Despite the plethora of haptic devices available and the abundance of applications for which haptic feedback can benefit user experiences, the widespread adoption of haptic technology to this day remains largely confined to the primitive vibrations found in handhelds such as controllers and smartphones. Attempts to bring more sophisticated haptic devices to market, such as tabletop displays and haptic gloves, have either struggled to attain broad appeal or aspired only to serve niche industrial and academic roles. The issue is not one of technological deficiencies, but rather an unconvincing value proposition, as it is typical for these device to be both expensive and highly specialized for particular use-cases.

To this end, the field of haptics has recently shifted toward a more pragmatic approach. Researchers are now investigating ways of creating compelling experiences with low-cost actuators and novel modalities. To expand the appeal and utility of haptics, devices in *wearable* formats have emerged. The term *wearable haptics* generally encompasses devices such as bracelets, armbands, sleeves, and even entire garments. Haptic gloves, although wearable, are typically classified separately.

In contrast to world-grounded desktop devices, body-grounded wearables can be generalized to many different tasks and applications. They have been successfully utilized in common haptic scenarios such as navigation and guidance [5], [6], text communication and notifications [7], and augmented and virtual reality (AR/VR) interactions [8]. Another promising application area is in providing tactile and kinesthetic grasping feedback for upper limb prosthesis users [9] and ultimately integration with advanced myo-electric control [10]. With respect to general robotics applications, wearables have been used to mediate human-robot interaction in cooperative tasks [11] and provide an elegant solution for delivering feedback during robotic teleoperation [12]. This is especially true in safety-critical situations such as robotic surgery where the addition of haptic feedback to the control interface introduces stability issues [13]. Depending upon the implementation, a single haptic wearable could conceivably offer all of these capabilities and more. It is not hard to imagine a future where all-day wearable haptics are tightly integrated with other mobile technologies such as smartphones, smartwatches, and eventually AR glasses.

Manuscript received November 29, 2021; accepted March 1, 2022. This work was supported by the Reality Labs Research through an Sponsored Research Agreement with Rice University. This paper was recommended for publication by Associate Editor G. Venture and Editor M. Yim upon evaluation of the reviewers' comments. (Corresponding author: Evan Pezent.)

Evan Pezent, Priyanshu Agarwal, Jessica Hartcher-O'Brien, and Nicholas Colonnese are with the Reality Labs Research, Redmond, WA 98052 USA (e-mail: epezent@fb.com; pagarwal18@fb.com; jesshartcher@fb.com; ncolonnese@fb.com).

Marcia K. O'Malley is with the Mechatronics and Haptic Interfaces Laboratory, Department of Mechanical Engineering, Rice University, Houston, TX 77005 USA (e-mail: omalley@rice.edu).

Color versions of one or more figures in this article are available at <https://doi.org/10.1109/TRO.2022.3164840>.

Digital Object Identifier 10.1109/TRO.2022.3164840

Before such a device can be realized, important questions and design choices must be considered.

1) *Where should an all-day wearable device be worn?* The wrist is the sensible choice. Though the design space is more restricted than that of an armband or sleeve, technology-integrated wristbands and bracelets are well established commodities, socially acceptable [14], and sometimes even fashionable [15]. Unlike garments, wristbands do not require frequent changing or cleaning. Furthermore, a precedent for haptic bracelets already exists, with smartwatches and now *social touch bracelets* (e.g., HEY Bracelet and Bond Touch) beginning to integrate basic haptic feedback.

2) *Which haptic modalities are both compelling and viable?* The majority of today's wearable haptic devices continue to leverage simple vibrotactile feedback. This is an obvious choice since vibration is a ubiquitous feedback primitive, and vibration actuators are usually inexpensive, low power, and easily controllable. For this reason, multiactuator vibrotactile *arrays* are common in haptic research devices. More exotic skin-contact-related modalities also exist, including squeeze [16], stretch [17], shear [18], twist [13], [19], thermal [20], and electrical [21] stimulation. There is strong evidence to support the *multimodal* combination of one or more of these modalities with vibrotactile feedback, and this is perhaps one way in which wristband devices can be made more applicable to complex applications such as AR/VR interactions. Multimodal haptics offer the ability to target different mechanoreceptors in the skin, enabling higher rates of information transfer to users [22] or more realistic simulation of virtual events [8], [23]. However, it is not practical for a device to implement all modalities, nor advisable since they are easily confused [22], [24]. Squeeze, stretch, shear, and twist are all similar in that they apply localized topical pressures to the skin. The latter three offer bidirectional stimulation, which in theory could provide an advantage to navigation or tasks requiring large cue sets. Unfortunately, these three modalities require consistent skin contact through friction [17] or adhesives [19], a matter which is complicated by skin moisture, the environment, and prolonged use. Thus, squeeze appears to be the most practical choice and is certainly the most researched. Squeeze feedback is thought to be less attention demanding than vibration [25], provides more intimate feedback similar to how one human might attract the attention of another [16], [26], and may elicit affective or emotional responses [27]. Squeeze has additionally been identified as a strong candidate for providing proportional kinesthetic information (e.g., grasp force [18], [28]).

3) *Are compact wearables possible with current technology?* The primary limiting factors of any wearable haptic device are usually actuators and sensors, whether in regard to their size, weight, cost, or power consumption. With the exception of vibrotactile feedback, all modalities discussed thus far typically rely on either bulky servos or pneumatic systems. In addition to size concerns, the power requirements for these types of actuators are often high, which poses a significant challenge to ultimately operating entirely on battery power. Engineers will need to resort to clever and efficient mechanisms to compactly integrate current actuators until the day that more ideal actuators and materials are readily available [29]. The control of these actuators is not a trivial matter either, as variations in limb



Fig. 1. Tasbi is a compact multimodal haptic wristband capable of delivering vibrotactile feedback at six locations and uniform squeeze feedback around the wrist (tethering cable not shown).

geometry, tissue impedance, and posture degrade the consistency of haptic feedback. Advanced sensing capabilities can mitigate these issues, but potentially increase the cost and size of the device. While there are other important aspects not discussed here (e.g., wireless communication), clearly there are already significant challenges to realizing compact haptic wearables.

In this article, we describe **Tactile And Squeeze Bracelet Interface (Tasbi)**, a multimodal haptic wristband (Fig. 1) that incorporates traditional vibrotactile actuation with robust wrist squeeze in a compact form factor. An early version of Tasbi was initially detailed in [30], and as such, this article offers several novel extensions. Notably, these include 1) a redesign of the device to include integrated force sensing, 2) the development of an instrumented wrist apparatus and force application tool to calibrate sensing, 3) the development of a novel closed-loop force control scheme and its characterization, and 4) three unpublished user studies that leverage our closed-loop force controller to quantify fundamental psychophysics related to wrist squeeze.

The rest of this article is organized as follows. In Section II, we survey the current landscape of haptic bracelets and discuss critical points that led to Tasbi's development. An in-depth look into the bracelet's latest design is provided in Section III, with emphasis on a novel squeeze mechanism that affords Tasbi high force output in a small package size, as well as the new addition of force sensing capabilities. In Section IV, we discuss methods and challenges to squeeze control, and demonstrate for the first time accurate and high-performance closed-loop control of wrist squeeze using inexpensive capacitive sensors. Leveraging Tasbi's unique force control abilities, we present the results of new psychophysical studies in Section V that highlight user sensitivity to wrist squeeze forces as well as its potential impact on vibrotactile identification and user comfort. Finally, Section VI concludes this article.

## II. BACKGROUND

A number of research groups have explored haptic feedback on the wrist and forearm area, with vibration and squeeze

modalities being by far the most common. Here, we survey designs and research results related to both modalities, and highlight findings that influenced the design of Tasbi. Additionally, we identify gaps in the literature that we aim to address with this article.

### A. Vibrotactile Bracelets

Generating vibration cues is most often accomplished through the use of small vibration motors (vibrotactors or factors). Types of vibrotactors include eccentric rotating masses (ERM), linear resonance actuators (LRA) or voice coils, or piezo actuators. Many researchers have investigated placing vibrotactors on the wrist and arm [31]. Because the wrist and arm provide ample surface area, the most interesting work usually employs *vibrotactile arrays*, i.e., two or more independently controlled vibrotactors, as a means of increasing information transfer. Two possible configurations exist—planar grid arrays or radial arrays.

Oakley *et al.* [32] studied a  $3 \times 3$  planar configuration on the dorsal side of the wrist. The results of their experiments showed that subjects more easily localize vibrations when they are presented perpendicular to the axis of the arm and inline with the wrist strap as opposed to along the length of the arm. They further showed that localization is improved by placing vibrotactors near bodily landmarks, such as the edges of the arm. Using a similar  $3 \times 3$  planar configuration, Chen *et al.* [33] compared placing the factors on the dorsal versus the volar side of the wrist. Their results agreed with the findings of Oakley's study with regard to direction and bodily landmarks, but they did not find a significant difference in localization between the dorsal and volar sides of the wrist. Paněls *et al.* [34] studied a circular planar configuration, but noted difficulties in identifying the actuated factors.

Matscheko *et al.* [35] compared arranging four factors in a planar grid on the dorsal wrist versus radially around the wrist. They showed that subject performance was best for the radial configuration in a memory and distraction task, and logically concluded that this was the result of spreading the factors farther apart. Following their advice, Carcedo *et al.* [36] tested variations of a band with 3, 4, 5, and 6 radially spaced factors. The results showed identification rates above 90% for the 3 and 4 factor configurations, and around 80% and 70% for the 5 and 6 factor configurations, respectively. Gupta *et al.* [37] developed a device with four radial voice coil actuators to enhance manipulation feedback of a touch screen surface, and Pece *et al.* [38] have developed a variation of voice coil technology that indents instead of vibrates the skin. The designs presented so far did not attempt to isolate vibration transfer between adjacent motors, which probably has a nontrivial impact on localization accuracy. Hong *et al.* [39] addressed the issues of vibration transfer by separating radially spaced factors with thin elastic thread. They concluded that in this configuration, up to eight factors can increase accuracy in a guidance task. All devices are summarized in Table I, and in general, it would seem that a safe bet for vibrotactile wrist bands is to incorporate at least four factors in a radial configuration.

One unresolved question from these studies regards the importance of mechanical coupling between factors and skin,

TABLE I  
VIBROTACTILE BRACELETS

	Actuators	Configuration
Oakley [32]	9 LRA	Planar
Chen [33]	9 LRA	Planar
Lee [42]	3 LRA	Planar
Matscheko [35]	4 VC	Planar/Radial
Carcedo [36]	3-7 ERM	Radial
Gupta [37]	4 VC	Radial
Hong [39]	4/8 ERM	Radial
Pece [38]	4 VC (indenting)	Radial

ERM = eccentric rotating mass; LRA = linear resonant actuator; VC = voice coil.

and whether localization accuracy improves and degrades with increasing coupling force. This article presents some insights toward this in Section V. While identification accuracy is indeed important for discrete information transfer, we should not necessarily use these results as a driving factor when designing bracelets for AR/VR interaction. For one, vibrotactors are inexpensive and consume small amounts of power, and including more than perceptually identifiable is not of high concern—we can always use a subset of the available factors when identification accuracy is needed. The reason we may choose to include redundant factors is to achieve smoother transitions when presenting continuous spatial patterns, i.e., blending the vibrations of adjacent factors to create *apparent motion* [40], [41].

### B. Squeeze Bracelets and Armbands

While vibration has been extensively studied for decades, squeeze or compression feedback has only become of interest to the haptics community within the past few years. There are many reasons for investigating squeeze. First, while vibration primarily excites Pacinian nerve endings, squeeze can innervate the slower adapting Merkel and Ruffini receptors [43]–[45]. Zheng and Morrell argued that squeeze, compared to vibration, is less attention demanding and more appropriate for ambient feedback [25]. Along these lines, Baumann *et al.* [16] suggested that squeeze provides intimate feedback that more closely resembles social touching behaviors, and have further used squeeze to elicit affective emotional responses from users [46]. Nakamura *et al.* [27], [46] developed a squeeze-like device that applies four normal forces to generate the hangar reflex at the wrist [47]. Important to AR/VR applications, squeeze has been demonstrated to be more appropriate for providing *continuous* feedback, in contrast to the discrete alert-type buzzes vibration offers. As such, squeeze has also been used to communicate grasping forces for prosthetic [48] and teleoperated applications [49].

Though some squeeze devices have been developed specifically for the wrist, many have been deployed to the forearm or bicep (Table II). Most squeezing devices employ electromechanical servos or DC motors to tension flexible bands around the limb [20], [49]–[51], and are characterized by generating both *normal* and *tangential* forces on the skin. Noting that tangential forces provide another haptic feedback modality, i.e., skin stretch, some designers have included two or more actuators so that squeeze and stretch can be actuated independently and simultaneously [18], [28], [52]. However, Zook *et al.* [24] and

TABLE II  
SQUEEZE BRACELETS AND ARMBANDS

Stanley [50]	wrist	belt	1 servo	-	pos.
Brown [49]	wrist	belt	1 servo	-	pos.
Bianchi [52]	wrist	belt	2 motor	2 enc.	pos
Song [20]	wrist	belt	1 servo	-	pos.
Meli [28]	forearm	belt	4 servo,	-	pos.
Wang [51]	bicep	belt	1 servo	-	pos.
Casini [18]	bicep	belt	2 motor	2 enc.	pos.
Treadway [48]	bicep	belt	1 servo	-	pos
Gupta [57]	wrist	SMA	3 SMA	-	curr.
Chinello [54]	forearm	clamp	3 servo	3 FSR	force
Moriyama [55]	wrist	clamp	4 servo	-	pos.
Sarac [56]	wrist	clamp	2 linear	2 enc.	pos
Pohl [45]	wrist	pneu.	custom	-	press.
Raitor [60]	wrist	pneu.	4 reg.	-	press.
Young [58]	wrist	pneu.	8 reg.	-	press.
Payne [61]	bicep	pneu.	6 reg.	2 FSC	force
Zhu [59]	forearm	pneu.	1 reg.	1 FSC	force

SMA, shape memory alloy; FSR, force sensing resistor; FSC, force sensing capacitor.

Fleck *et al.* [53] have demonstrated that squeeze and stretch cues perceptually interfere with one another and are easily confused by users. Consequentially, some devices attempt to isolate squeeze to only normal forces, and have used clamping mechanisms [54], linkage-based mechanisms [55], and linear actuators [56] to do so.

Gupta *et al.* [57] addressed the size concerns of the aforementioned devices by employing shape-memory alloys (SMAs), but this approach required high power (up to 30 W) and insulation to shield users from heat. Others have resorted to pneumatic-based compression. Pohl *et al.* [45] used pneumatically actuated bladders to create uniform compression akin to a blood pressure cuff. Young *et al.* [58] used eight small inflatable bellows to provide targeted squeeze around the wrist. Other instances of pneumatic actuation include Pneusleeve [59], WRAP [60], and a device from Payne *et al.* [61]. While these devices are both sleek and likely more comfortable due to their soft designs, pneumatic actuation is currently limited by bulky compressor technology. Some researchers have developed modular micro-compressors [62], [63] to power pneumatic devices, often worn on the waist or in a backpack. However, it seems very unlikely that consumers would be willing to wear a separate power source for an all-day wearable wristband. Thus, a traditional electromechanical approach will still be required for the near-term future.

An often overlooked facet of electromechanical squeeze feedback is the control implementation. It is typical for these devices to employ servo position control of the band-tensioning actuator. Thus, the amount of squeeze force delivered is inherently tied to the tissue impedance of the stimulus site. Sarac *et al.* [56] noted the limitations of this approach in their study for VR interactions, and attempted to resolve the issue by estimating applied force from the average impedance of hairy-skin. Control of contact forces is generally limited to pneumatic actuation where bladder pressure, and thus contact pressure, is controlled for using open-loop control. Closed-loop control on the forearm has been accomplished with custom force sensors as well [59], [61]. However, because pneumatic bladders necessarily change shape and size, there still remain some ambiguities as to what these devices are actually controlling for from a *perceptual* standpoint. Another challenge to force-control is in knowing

how much force is sufficient in the first place. All psychometric analysis of wrist squeeze, thus far, has been quantified in units that are inherently tied to the device (e.g., the amount of motor displacement, band-tension, or regulator-pressure). This article presents answers to these unresolved issues in Sections IV and V.

### C. Multimodal Devices

Most devices discussed so far were developed for notification-type feedback, and thus can only offer limited experiences complex applications such as AR/VR. One way in which wristband devices can be made more generalizable is by enabling *multimodal* feedback, or more specifically, integrating *both* vibration and squeeze into a single interface. Combining squeeze and vibration could not only provide a richer cue set with higher information throughput, but also the ability to convincingly depict virtual interactions that are inherently multimodal. This concept has been most prevalent in the development of glove interfaces for extended reality (XR) applications, where kinesthetic mechanisms and vibration actuators are combined to convey more realistic interaction.

Despite a high volume of research into vibration and squeeze feedback wearables alone, a relatively limited number of devices have implemented both modalities into a single wearable. Baumman *et al.* [16] developed a multimodal wrist device which featured squeezing and low-frequency tapping for emulating human attention getting practices. Dunkelberger *et al.* [7] developed the MISSIVE, which combines separate bands for vibration and squeeze. They successfully used the device to convey language through skin, and argued that this multimodal approach allowed them to render a larger set of distinguishable cues than would have been possible under a unimodal approach. Agravi *et al.* [64] presented a forearm device that incorporated squeeze and four tactors into the same band, but did not address the fact their design causes tactors to translate on the skin, which likely confuses users. None of these devices managed to achieve a design robust or compact enough for all day wearability. Finally, while Zook *et al.* [24] showed that squeeze interferes with skin stretch, it is not currently known if the same is true for squeeze and vibration. Thus, this article also attempts to answer this question in Section V.

## III. DESIGN

Upon examining the current landscape of wrist wearables, we set out to design Tasbi, a multimodal bracelet that combines vibrotactile feedback with radial squeeze haptics. The design process was driven by several considerations and constraints. Our primary goal was to build a highly compact unit with minimal sacrifices to actuation output and bandwidth. Based on commercial smartwatches, our target size was  $50 \times 50 \times 10$  mm with a total mass less than 200 g. We decided the device should emit little audible noise to avoid annoying users or interfering the haptic experience. To accommodate various modes of squeeze control, integrating both position and force sensing were desired. Actuator power consumption was constrained 2 W, so as to not dissipate an uncomfortable amount of heat and to reasonably remain within the capabilities of lithium-ion batteries. With that, it is important to note upfront that we did *not* aim to completely

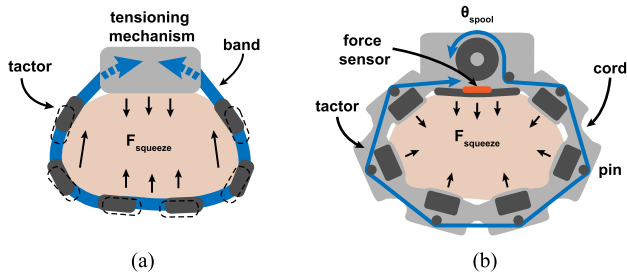


Fig. 2. (a) Typical constricting-band approaches to squeeze produce nonuniform and tangential forces which would cause embedded factors to shift. (b) Our decoupled approach aims to produce pure, uniform normal forces.

self-contain this iteration of Tasbi. Therefore, Tasbi does not include onboard microcontrollers, batteries, or wireless communication, and relies on an external control unit. We felt that it was more important to focus on miniaturizing the mechanisms and sensing for the initial prototype, and address these concerns in a future iteration.

#### A. Squeeze Mechanism

As already discussed, most squeezing devices use a similar scheme where one or more rotational actuators are used to directly wind a band element into an actuator housing [16], [18], [20], [28], [49], [50]. While this approach is straightforward, it presents two main issues [Fig. 2(a)]. First, directly tensioning the band itself gives rise to an unequal distribution of forces where there are concentrated tangential shear forces on the sides of the arm, and smaller normal forces on the underside. Furthermore, this results in nontrivial squeeze force losses due to friction between the band and skin. Second, because this method causes the band to translate along the skin, it is not well suited to embedding vibrotactile elements in the band since they would consequently translate too. Maintaining the radial positions of the vibrotactors is key since their movement would decrease user identification rates and possibly cause discomfort. Some devices have circumvented this issue by using two separate bands: One for generating squeeze, and one for housing vibrotactors [22]. However, this approach is less than ideal for a wrist-watch form factor and complicates donning and doffing the device.

Tasbi solves these problems by decoupling squeeze actuation from the wrist band and vibrotactors. This is accomplished by means of small diameter, flexible ultra-high-molecular-weight polyethylene (UHMWP) cord (trade name Dyneema/Spectra), which wraps circumferentially around the exterior of the band [Fig. 2(b)]. Tensioning this cord, not the band, creates squeeze forces. Friction is minimized by separating contact between the cord and band with smooth, polished steel pins placed directly above each vibrotactor. This mechanism results in cord tension being transmitted as an inward force approximately normal to the vibrotactor, as can be understood through simple geometric inspection. Because friction between the pin and cord is small, little tangential force is transmitted to the band, and as a result each vibrotactor maintains its radial position around the circumference of the wrist. Eliminating friction and tangential forces also allows for a smaller actuator, since most power is ideally converted to purely normal squeeze force. Furthermore,

tensioning the lightweight cord instead of the entire band means less mass must be moved to accomplish similar displacement, further reducing the power required of the tensioning actuator.

A rudimentary prototype of the squeeze mechanism and haptic sketching [65] suggested that approximately 10 N of tension would be required to achieve an appropriate range of squeeze stimuli. Several tensioning mechanisms and actuators were initially considered. For ease of implementation and control, an electromechanical approach, as opposed to pneumatic or other exotic approaches, was decided. Linear actuation methods were disregarded since achieving a stroke length necessary to generate enough cord takeup would necessitate a nonideal housing length. For this reason, a rotary scheme with a winding spool was chosen. Many hobbyist servo motors met our size and torque requirements, but generally these actuators produce a high degree of audible noise and do not provide continuous rotation. We therefore chose to use a brushed dc motor. An additional reduction stage was required to meet our torque needs. Commercially available gear units, which typically implement one or more serial stages of planetary gears, were found to also suffer audible noise issues and were unavailable in sufficiently compact sizes.

Our final solution utilizes a 12-mm Maxon DCX motor coupled to a 100:1, 13-mm strain-wave gear unit from harmonic drive in Fig. 3. These drives offered a set of characteristics we deemed necessary to fully realize Tasbi: 1) a sufficiently high torque reduction; 2) low audible noise due to having zero mechanical backlash, and most importantly; and 3) compactness far superior to conventional gear units. The dc motor and harmonic gear unit are contained within a  $50 \times 35 \times 15$  mm housing (below our target size), which rests on the dorsal side of the user's wrist. Attached to the output of the gear unit is a 10-mm diameter spool. Both ends of the cord terminate to the either side of the spool so that the take-up rate is doubled (anecdotally, it is possible to double cord tension at the expense of half the take-up rate by fixing one end of the cord to the housing, achieving a pulley-like effect). The cord is redirected internally over additional smooth pins to exit at the center of the main housing, balancing a moment arm that would otherwise cause the housing to torque about its short axis.

The dc motor is driven by an externally located 4-quadrant pulse-width modulation (PWM) servo controller (Maxon Escan 24/2) operating in a current control mode. Position estimation is achieved via incremental encoder feedback placed on the motor side of the mechanism. To maintain a small footprint, we used an ultra miniature optical encoder (Elasta E OI R016) featuring a reflective mirror code wheel, with the optoelectronic sensor PCB embedded into the rear connector panel of the housing. With 128 counts per revolution and a 100:1 reduction, Tasbi can achieve  $0.007^\circ$  positional accuracy at the spool output in 4X quadrature mode. This level of accuracy is unnecessary for spool positioning, but provides smooth velocity estimation which was ultimately critical to our squeeze control implementation (see Section IV).

It is worth noting that the drive mechanism is not easily back-driven due to its high gearing ratio. While this does present mild safety concerns (i.e., users cannot manually loosen the device with ease), it means that Tasbi can maintain varying levels of

squeeze without continuous input from the motor. For example, the motor can be used to squeeze to a desired level, turned OFF, and then friction in the gear unit will hold the squeeze level. This property may eventually prove beneficial to self-contained versions of Tasbi and similar devices where battery power must be conserved.

Readers familiar with tendon routing mechanism might understandably be skeptical to the long-term viability of the cord-based mechanism presented here. Indeed, early versions of Tasbi [30] were prone to internal snagging and spool disconnection. Subsequent revision eliminated these issues. Over a dozen Tasbi prototypes have been fabricated and deployed at Rice University and Reality Labs Research, and no failures have been reported thus far. One unit in particular has been used for well over a year for demonstrations and over 100 h of device and subject experimentation without any issue.

### B. Squeeze Force Sensing

Enabling Tasbi with squeeze-force sensing was one of the more challenging aspects of the design. To simplify the process, we made the assumption that placing a single sensor in the main housing would accurately capture gross squeeze force around the entire wrist. This assumption can be made due to the way in which Tasbi equally distributes forces [see Fig. 2(b)], which is experimentally shown in Fig. 6.

Because a significant portion of the main housing was already consumed by the tensioning mechanism, integrating a traditional single-axis load-cell was ruled out due to space constraints. Therefore, we only considered force sensors with a thin-film or sheet-like form factor. Force-sensing resistors (FSR) are a technology that typically falls under this category, but are notorious for exhibiting signal drift and hysteresis issues. A similar, yet relatively newer technology, force sensing capacitors (FSC), has been shown to provide improved sensitivity and repeatability compared to FSRs [66] at the expense of requiring more sophisticated electronics and signal conditioning. The most readily available FSCs are the SingleTact sensors from pressure profile systems (PPSS).

Tasbi incorporates an 8-mm diameter, 10-N SingleTact FSC sensor, located between the underside of the main housing and a bottom plate in Fig. 4. Two important design choices were made to ensure that the majority of force seen at the skin interface is transmitted through the sensor head. First, the bottom plate is held in compression with four springs and screws located at each corner of Tasbi's housing. This allows the plate to be carefully fastened until just a slight amount of preload is measured by the sensor. Second was the design of the bottom plate itself, which 1) has an extended contact surface to mitigate issues that arise with skin deformation under load, and 2) is made from a flexible ABS plastic with intentional material removal to give it a leaf-spring like characteristic. The SingleTact electronics PCB is integrated directly into Tasbi's housing, and transmits the force measurement as an analog voltage through Tasbi's connector interface. Overall, our experience with SingleTact's FSCs has been good. The sensors display some manageable hysteresis, but no significant drift. Interestingly, their sensitivity is good

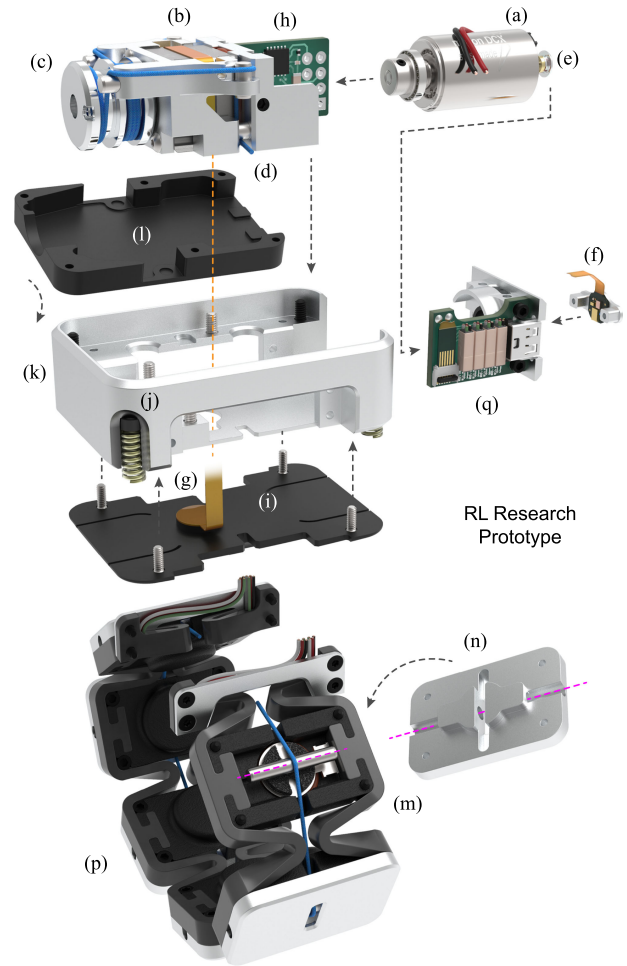


Fig. 3. Tasbi exploded view—the squeeze mechanism consists of a (a) 12-mm dc motor and (b) a 13-mm harmonic drive gearbox, (c) which drives a two-sided spool (d) to create tension in a UHMWP cord. Spool position feedback is provided through an optical encoder consisting of (e) a reflective code wheel and (f) optoelectronic sensor. Squeeze force feedback is measured via (g) a force-sensing capacitor and (h) signal conditioning PCB. The force sensor is held in light compression against (i) a bottom plate (j) with four corner springs. The drive assembly (k) drops into the main housing and (l) is secured in place with a housing lid. (m) Each vibrotactor unit contains a 10-mm LRA vibrotactor and a smooth stainless steel pin to convert cord tension into normal force. Vibrotactor units are (n) clipped into elastic sidings and (o) secured with lids. (q) All signals and power to and from Tasbi are transmitted over a micro-HDMI cable that connects to an internal breakout PCB.

enough that it is possible to detect some user's heartbeat from the force measurement when Tasbi is sufficiently tightened.

### C. Vibrotactile Band

Tasbi's wrist band contains six vibrotactor units. Each unit consists of a plastic housing in which the vibrotactor is fit. The vibrotactors are generic 2.5-VAC, 10-mm linear resonant actuators (LRAs) with an nominal frequency range of 150–200 Hz. Because each tactor's performance is sensitive to fitting tolerances, we used two O-rings to achieve a snug but not overly tight fit into the assembly in Fig. 5. The tactor is secured axially with a foam layer and the housing lid. Along the underside of the lid is a press-fit hole for one of the aforementioned smooth pins. The distance from skin to the pin was optimized

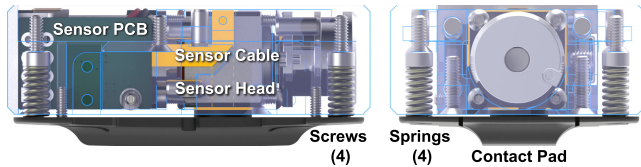


Fig. 4. Tasbi force sensor—a SingleTact 8-mm, 10-N force-sensing capacitor is sandwiched between the main housing and a plastic bottom plate. The plate is held in compression through four compression springs and screws so that the sensor experiences minimally preload.

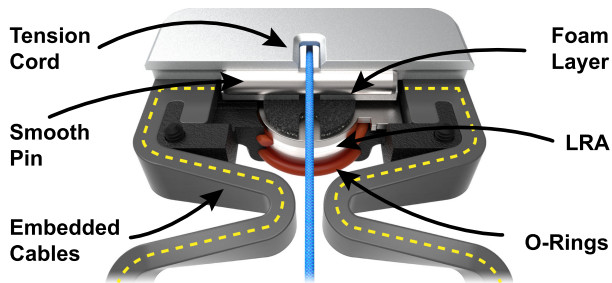


Fig. 5. Tasbi vibrotactor assembly—the tactor is secured into the lower plastic housing via two O-rings and a foam layer. The metal lid contains a press fit smoothpin over which the tension cord slides. Tactor power cables are embedded within the 3-D-printed band sides in a postprocessing step.

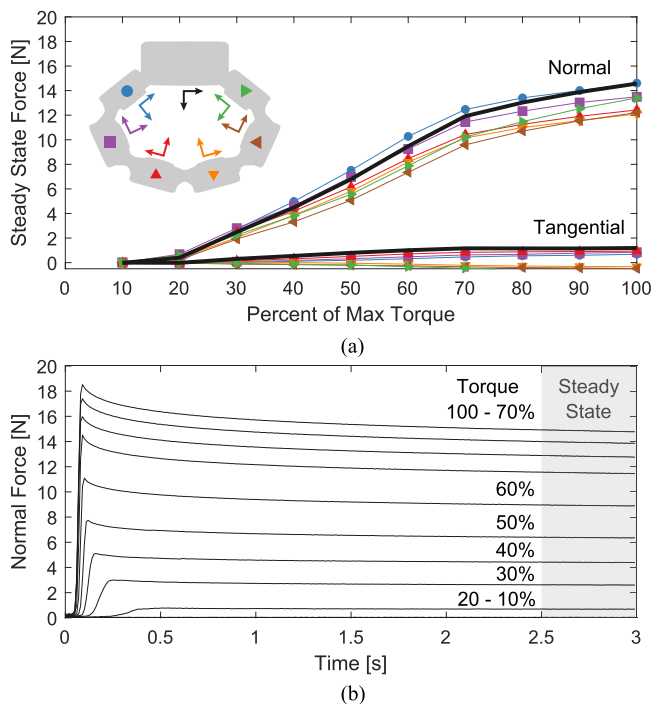


Fig. 6. (a) Steady-state normal vs. tangential forces under each vibrotactor module and the main housing as a function of commanded motor torque. (a) Representative responses for each torque step under the main housing.

so that the tensioning cord would clear and not rub against the user's skin.

Each tactor unit is clipped in between polyurethane rubber sidings via T-shaped joints. Tactor power cables are embedded within the rubber siding and enter the main housing through openings on both sides. The elasticity and geometry of the

sidings, inspired by the commercial Myo armband, allow the band to be stretched over the user's hand during the donning and doffing process while also reducing vibration transfer between adjacent tactor units, similar to the device in [39]. Tasbi has a nominal inner circumference of approximately 150 mm, equal to the 50th percentile female wrist circumference. Thus, for most users, the band provides a light amount of passive squeeze to ensure a comfortable initial fit.

Vibrotactor control is accomplished using the Syntacts vibrotactile framework, which leverages audio interfaces to control high-density tactile arrays with low latency. In our implementation, we interface the framework with a MOTU 24Ao sound card, which connects to a Syntacts amplifier board housed in the Tasbi control unit. Using Syntacts, it is possible to generate a wide variety of waveforms, both discrete and continuous, that can be played on individual or multiple tactors. Possible waveforms can be composed from simple oscillators (e.g., sine, square, saw), amplitude and frequency modulation, amplitude-shaping envelopes, and track-based sequences. Syntacts also provides a spatializer mode that treats the tactors in Tasbi's band as a continuous space where amplitudes of adjacent tactors are blended. To achieve the lowest latency possible (<4 ms), we use Stienberg's ASIO sound driver with Syntacts. We point the reader to [41] for more details regarding the Syntacts' framework and amplifier board design.

#### D. Power and Control Unit

As previously mentioned, all power and control is done through a custom external unit. This control unit houses linear dc power supplies (so to avoid noise associated with common switch-mode power supplies), a PWM servo controller for the dc motor, and a multichannel Syntacts amplifier for the vibrotactors. It is important to note that the Syntacts amplifier, which was developed in conjunction with Tasbi, leverages linear class AB amplifiers to further minimize electrical noise in the overall system (see [41] for more details). Each Tasbi connects to its own control box via a standard micro-HDMI cable (an unconventional choice, but one of the few interfaces providing the necessary pint count and form factor). With the exception of vibrotactor input signals, all digital and analog signals between the control box and the host PC are done over a Quanser Q8-USB sampled at 1000 Hz.

## IV. SQUEEZE CONTROL

The majority of devices leverage squeeze for general purpose cues, notifications, or predefined effects [20], [22], [59]. With Tasbi, we additionally aim to accommodate virtual hand and finger interactions in AR/VR (see [30]), which requires more sophisticated real-time control. As such, the following requirements were specifically set forth during the development of Tasbi's squeeze controller:

- High dynamic range: The controller should be able to produce low and high output to convincingly convey the wide range of forces that arise from virtual interactions.
- Fast response times: The controller should be robust to the unpredictability of user interaction, which may present

scenarios where squeeze must rapidly change from low to high output in a moment's notice.

- **Accurate tracking:** The controller should be able to accurately track continuous, real-time variables.
- **Smooth operation:** The controller should be perceptually free of mechanical noise so that users do not confuse squeeze for vibration stimuli.
- **Consistent stimuli:** The controller should produce perceptually equivalent stimuli for a given input regardless of hand posture or wrist impedance.

The following sections present and discuss the progressive process of developing and characterizing a closed-loop squeeze controller which fulfils these requirements.

### A. Torque Control

At the lowest level, squeeze can be produced through simple open-loop torque control of Tasbi's tensioning motor using only the ESCON servo-controller in current control mode. Fig. 6 shows the relationship between motor torque and contact force at the bracelet–wrist interface. We note significantly higher production of normal force than tangential force, and that the force produced under the housing and each tactor housing is quite comparable [Fig. 6(a)]. Both points validate Tasbi's unique tensioning mechanism, presented in the previous section (see Fig. 2). Tasbi can generate steady-state forces as high as 15 N, though it can also be seen that more distal tactor modules have a slightly lower normal force than proximal modules, which is likely due to cord tension loss between adjacent modules as a result of pin friction.

However, Fig. 6 also illustrates two challenges for open-loop torque control: 1) Torque levels below 15% max torque produce little to no force output, revealing dead band in the tensioning mechanism due to friction in the drive components; and 2) torques above 50% display a noticeable relaxing effect, most likely due to the material properties of the tensioning cord.

Even if these issues could be overcome, torque-only control is fundamentally flawed because it presents no means to deescalate squeeze force due to nonmonotonic behavior. While it is possible to produce increasing levels of squeeze force by ramping torque, it is not possible to reverse force by decreasing torque because wrist impedance is incapable of backdriving the tensioning mechanism. Thus, a closed-loop control scheme is required.

### B. Position Control

Our first approach to closing the loop on squeeze was through position control of the tensioning spool. Such a controller is trivially implemented with feedback from the incremental encoder on the motor side and a proportional-derivative (PD) control law. In this mode, a range of squeeze stimuli is produced by controlling the squeeze mechanism between a minimum and maximum spool position. The range is determined *in situ* by recording the steady-state position when open-loop torque is held at the minimum level (i.e., 15%) and the maximum level (i.e., 100%). This range was different for individuals, but typically between 40° and 60° of rotation

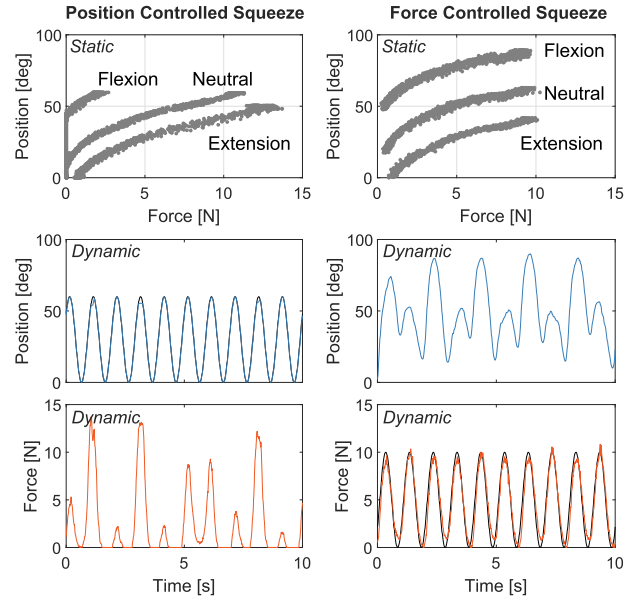


Fig. 7. Impedance of the wrist changes considerably with posture. In the top two plots, measurements of force and spool position are shown for static wrist poses while either a (left) sinusoidal position or (right) force trajectory is controlled for. Clearly, we cannot assume a consistent relationship between squeeze force and spool position. The bottom four plots show the dynamic case as a user cycles between full extension and flexion. Though position control is accurately maintained during hand movement, the delivered squeeze stimulus changes drastically (bottom left). Thus, we require direct control of squeeze force (bottom right) if we hope to deliver consistent stimuli to users.

Because motor position control is simple and practical, this is the most common approach used by servo-actuated squeeze devices. Indeed, we have made abundant use of position-controlled squeeze with Tasbi, and the controller works well enough for demonstrations and short-lived uses. However, a number of issues plaguing position controlled squeeze make it unsuitable for long term and general use. First and perhaps most importantly is that controlling for spool position offers no means to provide a consistent perceptual stimulus across users because it is inherently coupled to the impedance of the user's wrist. For example, 30° of spool rotation likely feels different for a person with tone wrists than it does for a person with soft wrists. Additionally, it can also feel different to an individual if the bracelet shifts along the arm, which is unavoidable. The issue is exacerbated by drift and/or creep in the cord tensioning mechanism, such that a given spool rotation does not produce the same amount of cord deflection over time. Finally, wrist impedance changes drastically with hand and finger posture, which negatively impacts the performance of position-controlled squeeze. In the left column of Fig. 7, Tasbi is commanded to track a sinusoidal position trajectory between 0° and 60° as an individual cycles through various wrist poses. Although nearly perfect positing tracking is maintained, the actual amount of delivered squeeze force changes significantly.

### C. Force Control

Based on the aforementioned issues with position-based control, it is clear that squeeze should be controlled through a

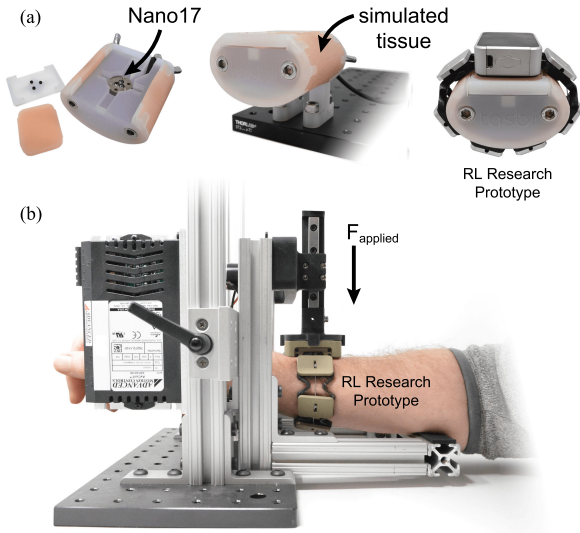


Fig. 8. Apparatuses. (a) The instrumented wrist integrates a high-accuracy ATI Nano17 force sensor and silicone-based simulated tissue. It served a critical role during the force controller development and tuning phases. (b) While general purpose calibrations of Tasbi’s integrated force sensor can be obtained with the instrumented wrist, an actuated calibrator facilitated customized calibrations to individuals by applying a known load through the bracelet. It was primarily used prior to the psychophysical experiments in Section V to ensure accurate reporting of force.

variable directly related to the contact mechanics between the bracelet and skin. Two choices include the amount skin indentation or the applied force or pressure. Because it is not yet clear which stimulus is more perceptually important at the wrist, and the complexities of implementing sensors for the former, we chose to explore direct control of the contact force between Tasbi and the skin. The implementation of force-based squeeze was considerably more involved than the previous methods, and so a detailed description of our approach follows:

1) *Sensor Calibration*: Prior to implementing any sort of force control, the force sensing capacitor in Tasbi needed to be accurately calibrated postinstallation to account for 1) sensor offset from the center-line of the main housing, and 2) non-negligible force leakage through the pressure plate compression springs. To this end, we fabricated two apparatuses to perform sensor calibrations, both endogenously and exogenously (Fig. 8).

The first apparatus was an instrumented wrist cross section with an integrated ATI Nano17 transducer that measures force along the axis perpendicular to Tasbi’s underside [Fig. 8(a)]. To reasonably simulate tissue mechanics, a 5-mm thick, molded silicone “skin” layer surrounds the outside of the wrist. We used SmoothOn Ecoflex silicone (#00-30 Shore hardness), which has seen widespread use in simulating tissue for medical training and research [67].

To perform the calibration, the ATI Nano17 was first zeroed without any externally applied load. Next, a Tasbi was slipped over the instrumented wrist and tightened to a base level of squeeze by setting the motor torque to 15% of its maximum. After the motor quit spinning, Tasbi was zeroed for position, switched into the position-control mode, and commanded to track a compound sinusoidal trajectory for 10 s. Force measurements from the instrumented wrist sensor and Tasbi’s internal

sensor were recorded. The force data were related with a second-order polynomial, which provided a quality fit with  $R^2$  typically greater than 0.95. Fig. 9(a) illustrates the calibration process and the accuracy of Tasbi’s internal sensor after the fit is applied.

The instrumented wrist provides a general purpose calibration that can be associated with the device and subsequently used on individuals as-is. However, minor error in the calibration can be expected considering each individual’s wrist deforms slightly differently under load. Thus, to uphold the integrity of the psychophysical experiments presented later in Section V, we developed an alternative calibration apparatus to generate user-specific calibrations *in situ*. With this procedure, Tasbi’s force sensing capacitor is calibrated to a known-load transmitted through Tasbi’s housing and onto the wrist.

2) *Controller Implementation*: With a calibrated force measurement from Tasbi, we next began controller design. The primary challenge during the design process was in overcoming the low-precision and noisy analog signal from Tasbi’s internal SingleTact force sensor. The noise seen on the sensor is largely due to high-frequency interference from the PWM motor driver signal, though some inherent noise is associated with the sensors as well. Although we could have taken physical corrective actions (e.g., linear drivers, improved cable shielding, or leveraging the sensor’s I2C interface), we chose to attempt a software-only solution.

Much of the controller development took place with Tasbi placed on the instrumented wrist. Because the force reported by the instrumented wrist and Tasbi’s internal sensor are well correlated post-calibration, we found it particularly useful to first design the controllers by closing the loop with the much higher quality instrumented wrist force signal, and then apply the prototype controller to Tasbi’s force measurement (Fig. 9(b)). Three separate controllers were developed and tested.

Taking the simplest approach first, we applied a PD control law similar to what was done with the position controller:

$$e(t) = F_{\text{ref}}(t) - F_{\text{act}}(t) \quad (1)$$

$$\tau = K_p e(t) + K_d \frac{de(t)}{dt} \quad (2)$$

where  $F_{\text{ref}}(t)$  is the desired force,  $F_{\text{act}}(t)$  is the actual force measurement from either the instrumented wrist of Tasbi,  $e(t)$  is the force error,  $K_p$  and  $K_d$  are the proportional and derivative control gains, and  $\tau$  is the torque to be commanded to motor. Fig. 9(b) illustrates the design process. The controller was first roughly tuned using the instrumented wrist force measurement as the process variable (first column), then switched to use to the force measurement from Tasbi (second column). Clearly, the PD controller suffers when using the noisier feedback. The controller was stabilized by reducing the gains and filtering the force measurement with a median filter, but the tracking accuracy was limited, with the controller being incapable of reaching peak forces (third column).

The simple PD controller was next modified to include a feedforward term proportional to the desired reference force

$$\tau = K_p e(t) + K_d \frac{de(t)}{dt} + K_{\text{ff}} F_{\text{ref}}(t). \quad (3)$$

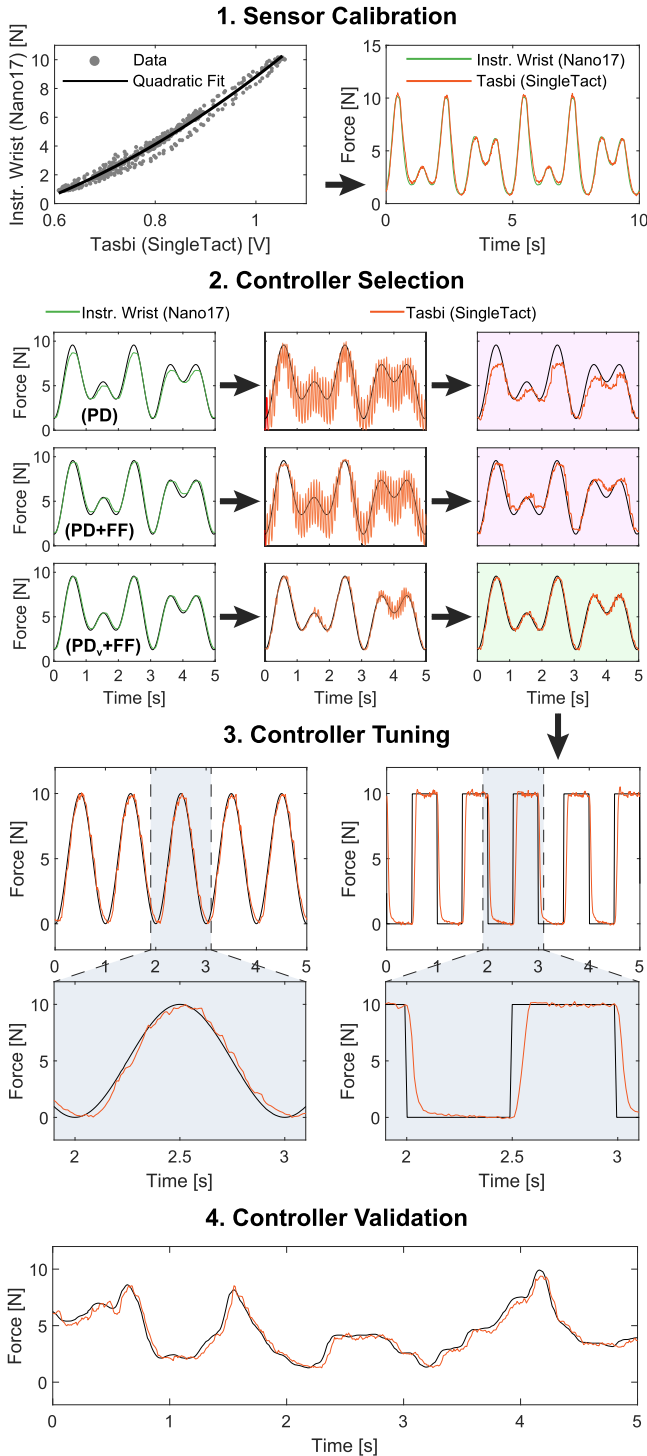


Fig. 9. Tasbi force controller development. (1) Tasbi’s internal force sensor is calibrated against the instrumented wrist’s Nano17. (2) Three controllers were tested by first closing the control loop with feedback from the Nano17 sensor, then applying the controller to Tasbi’s sensor and scaling the controller gains to stability. A feedforward and PD controller with the derivative term conditioned on *motor velocity* offered the best performance. (3) The PD<sub>v</sub>+FF controller was further refined to display RMSE less than 5% for a sinusoidal trajectory, and a rise time of 70 ms. (4) The final controller was validated in a VR context. Here, the controller renders the interaction force as a user jiggles a virtual button (see [30] or [8]).

The intuition here stems from knowing the relationship between squeeze force and torque (Fig. 6). Thus, we can predict the amount of torque required to generate a particular force and supplement the feedback partition with a portion of it. As shown in the second row of Fig. 9(b), the feedforward term greatly enhances the tracking accuracy of the simple PD controller. However, unacceptable tracking errors were still present. Ideally, we would have simply increased the value of the proportional gain  $K_p$  to eliminate the remaining tracking errors, with complementary increases to  $K_d$  to maintain stability. Unfortunately, since derivative action is taken on the backwards differentiated force error, this approach was too susceptible to noise to be viable.

If we maintain that the role of the derivative term is simply to dampen the action of the proportional term (which we wish to increase), we need not constrain the controller to using the derivative of force error, and can substitute it with a less noisy signal that is also proportional to the rate of squeeze. Thus, our final controller replaces the derivative term with *spool velocity*

$$\tau = K_p e(t) - K_{d,v} \frac{d\theta(t)}{dt} + K_{ff} F_{ref}(t). \quad (4)$$

With this simple modification, we can stably increase  $K_p$  to the point of eliminating tracking errors, provided an appropriate value of the new derivative gain  $K_{d,v}$  is set. In addition to eliminating tracking error, the herein referred to as PD<sub>v</sub>+FF controller also provides significantly smoother operation since it is not ridden with noise from the error derivative. Theoretical analysis on the stability of this “hybrid” control method is outside the scope of this article, but in practice, it has proven to be quite stable even at high frequency.

3) *Controller Characterization*: After refining the gains of PD<sub>v</sub>+FF controller and the median filter window width, the overall controller displayed a root-mean-square error (RMSE) of 0.48 N while tracking a 10-N, 1-Hz sinewave (< 5% error), and a rise time of 70 ms for a 10-N step response (Fig. 9(c)). The controller was subsequently validated across a variety of VR applications and on a number of individuals displaying different wrist characteristics. The controller also performed well regardless of the sensor calibration scheme, i.e., on the the instrumented wrist or *in situ* with the calibration applicator.

To further quantify the performance of the force controller, we benchmarked it against the position controller under the assumption that the latter drives the system near peak performance. Tasbi was placed on the instrumented wrist and commanded to track a sinusoidal force trajectory between 0 and 10 N. During this motion, the motor position was observed to consistently follow a trajectory between 0° and 40° [Fig. 10(a)]. We then performed a closed-loop system identification for both controllers, where the controller was commanded to track a 10-s Schroeder multisined excitation signal displaying a frequency range from 0 to 15 Hz [Fig. 10(b)]. The amplitude of the force trajectory was from 0 to 10 N, and the amplitude of the position trajectory was from 0° to 40°. Thus, both tests produced equal amounts of squeeze per Fig. 10(a).

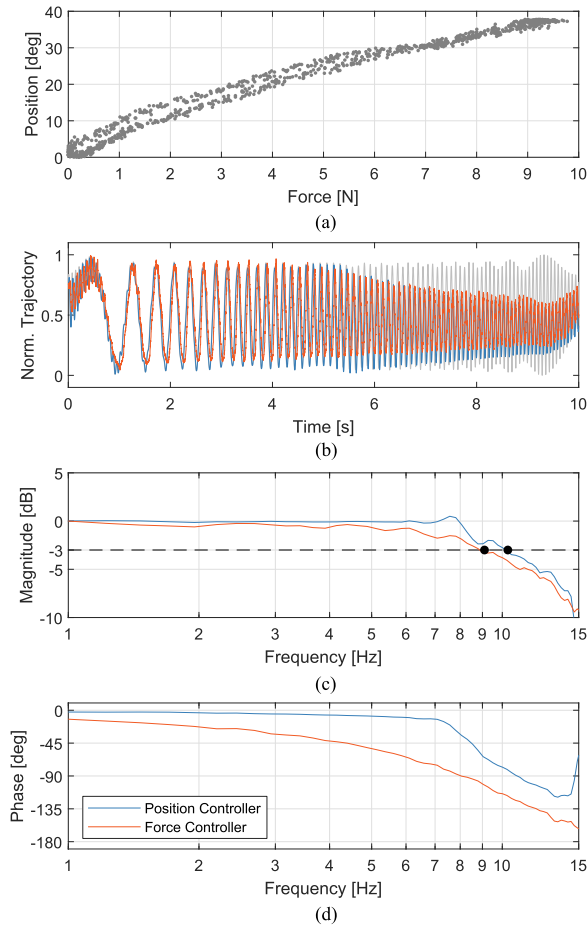


Fig. 10. Comparison of the position and force controllers. (a) Comparable ranges of squeeze and position are first identified, and (b) then the controllers are separately commanded to track an excitation signal within their determined range. (d) Although the force controller exhibits more phase lag, its overall bandwidth defined by the 3-dB cutoff is a quite comparable 9.1 Hz.

Fig. 10(b) shows both controllers attenuating near the 5-s mark. The Bode diagram in Fig. 10(c) and (d) shows that the force and position controllers display a surprisingly comparable bandwidth of 9.1 and 10.3 Hz, respectively. The phase diagram in Fig. 10(d) shows that the force controller lags considerably more than the position controller. This is not particularly surprising given the amount of filtering required to sufficiently smooth the force sensor signal.

The right column of Fig. 7 shows the extent to which the controller rejects external disturbances, where accurate tracking is maintained as the user cycles through various wrist orientations. More importantly, in contrast to the original position controller, the force controller provides a consistent stimulus regardless of wrist orientation or impedance.

#### D. Discussion and Future Improvements

The final squeeze force controller works considerably well given the simplicity of the sensors used and control law. Nonetheless, some limitations and room for future improvements remain. The primary challenge resides in accurately and consistently estimating the force at the bracelet–wrist interface.

Despite the good fit of the sensor voltage to measured or applied force, we find that this curve does shift slightly across several calibrations, particularly if Tasbi is not worn in the same location. We also observe that calibrations are not perfectly consistent across different individuals, thus necessitating the apparatus in Fig. 8(b). Ideally, we would like to eliminate this process, and perform only a single device-specific calibration. Our design made use of inexpensive and commercially available sensors, and so a custom force sensing capacitor that offers full coverage of the contact surface without force leakage and a higher resolution could significantly enhance the estimation of contact force. Other obvious improvements include better signal conditioning and electrical shielding.

Room for a more sophisticated control law exists as well. Although our final controller improves force control using supplemental state information from the optical encoder, we suspect that further improvements could be made using more a rigorous fusion of sensor data. For example, if a dynamic model of wrist impedance could be formulated, then samples from the force–position distribution [Fig. 7 and Fig. 10(a)] and/or the torque–force distribution (Fig. 6) combined with Kalman filtering might provide a more accurate and smoother estimation of squeeze force.

## V. PSYCHOPHYSICS

In this section, we characterize Tasbi in terms of human perceptual performance. The main contribution of these studies stems from Tasbi’s unique ability to control directly for wrist squeeze force. We quantify vibrotactor identification rates at varying levels of squeeze load (Study 1) as well as fundamental squeeze force thresholds for the wrist (Study 2). In addition, we quantify the maximum comfortable squeeze from a perceptual standpoint (Study 3). These studies have direct implications to not only Tasbi applications, but also to future device designs.

### A. Study 1: Vibrotactile Identification Accuracy

The first study aimed to characterize a user’s ability to successfully identify each of Tasbi’s six vibrotactors when actuated at random. The study was further designed to test if identification rates would be affected by different levels of static squeeze force and vibration stimuli duration.

1) *Subjects and Procedures*: In accordance with Rice University IRB Protocol #IRB-FY2020-43, we recruited 12 subjects (5 female, ages 21–33, mean 26). Each subject participated in both Study 1 and Study 2 in a single 90-min session divided by a short break. All subjects were naive to wearable haptics and had no prior training or experience with Tasbi.

Subjects completed Studies 1 and 2 by interacting with an on-screen graphical user interface (GUI) using a mouse with their right hand. Tasbi was worn on the right wrist, and each subject’s arm was supported such that Tasbi was suspended over free space and not inadvertently resting on any surfaces. To prevent use of visual or auditory information, a curtain occluded subjects’ view of Tasbi, and pink noise played over headphones throughout the experiments.

Following the experiments, each subject had their wrist dimensions measured at the Tasbi stimulus site (approximately 6 mm behind the styloid process). The means and standard deviations for wrist circumference  $C$ , width  $W$ , and height  $H$  were found to be  $185.7 \pm 13.6$  mm,  $55.7 \pm 5.1$  mm, and  $53.9 \pm 5.6$  mm, respectively. To analyze the effect of wrist size, subjects were evenly binned into either a *small wrist* group ( $C < 185$  mm) or *large wrist* group ( $C \geq 185$  mm).

2) *Experiment Design*: The experiment was divided into three blocks conditioned on the level of preload squeeze force (0.5, 5, or 10 N) for that block. At the beginning of each block, Tasbi tensioned to the target force and held that force via the closed-loop force controller presented in Section IV for the remainder of the block. The block order presentation was randomized between subjects so that each of the six possible orders were equally represented. Within each block, 240 vibration stimuli were presented. Each stimulus was characterized by the individual vibrotactor actuated, or the stimulus location (T1, T2, T3, T4, T5, or T6), and the duration of the stimulus (50 or 250 ms). The excitation signal was held at a constant frequency (170 Hz) and amplitude (2.5 Vrms), consistent with the nominal operating conditions of Tasbi's LRAs. The stimuli conditions were evenly distributed, and thus 20 repetitions of each actuator–duration pairing were presented in each of the three blocks. Subjects indicated the vibrotactor they identified as being played via the GUI, which displayed a 2-D schematic of Tasbi's vibrotactor wrist layout similar to that shown in the bottom right of Fig. 11. Subjects were given approximately 2 min to self-explore the Tasbi's vibrotactors using the GUI at the beginning of the experiment to help them internalize the GUI schematic in relation to the tactile stimuli.

3) *Results*: The main results are shown in Fig. 11 where the proportion of all subjects' responses under each condition are plotted as confusions matrices. The percentage of correct responses  $P_C$  is read along the diagonal of each matrix. Overall, we see an identification rate of approximately 67.8% across all conditions, consistent with the findings in [36] for a 6-tactor design. A few notable differences should be taken into consideration. First, we tested much shorter stimulus durations (50 and 250 ms versus 600 ms) which we felt represented a more likely range of stimulus duration. Second, because the 12 o'clock position on Tasbi is occupied by the squeeze tensioner housing, Tasbi's tactors are more densely packed than the device in [36]. However, the difference is likely offset by the fact that our test was conducted more distally from the styloid process (6 cm versus 3.5 cm) where circumference is larger. Indeed, a rough calculation of tactor-to-tactor spacing for both studies is a comparable 26 mm.

To further analyze the data, a three-way repeated measures ANOVA (6 locations  $\times$  3 force levels  $\times$  2 stimulus durations) was conducted with  $P_C$  being the dependent measure. The majority of groups passed the Shapiro–Wilk test for normality, and all groups passed Mauchly's test for sphericity. The main effect of stimulus location was found to be significant ( $F(5,55)=3.72$ ,  $p = 0.006$ ) and is evident in Fig. 11(g), where identification accuracy varies greatly from 53.0% to 74.9%. Collapsing the data across factors of force and duration and

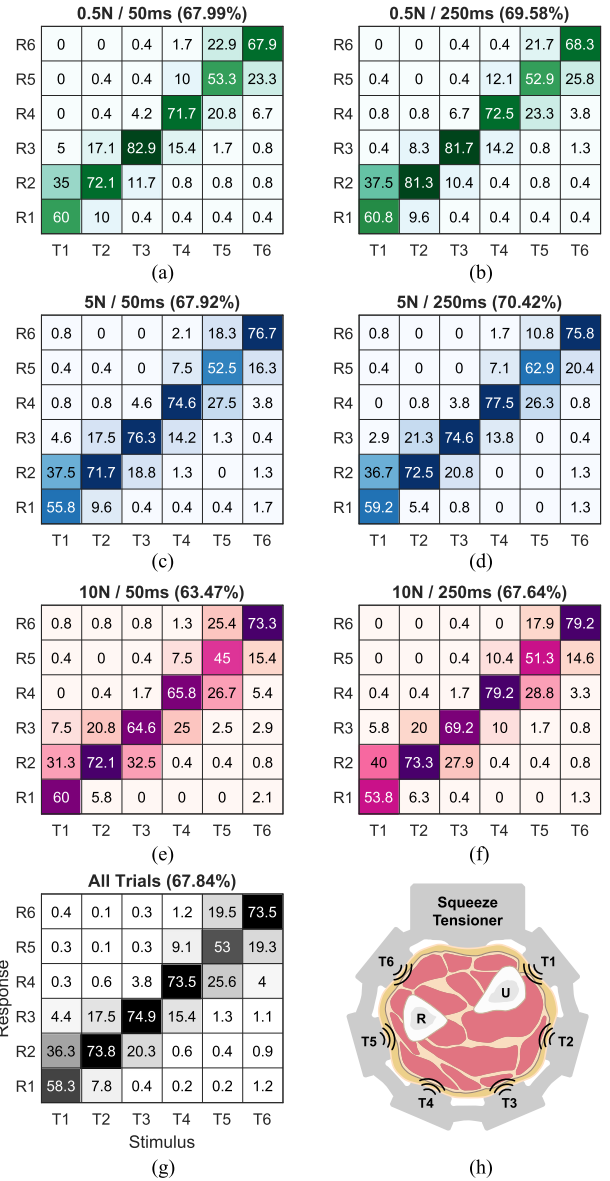


Fig. 11. Stimuli–response confusion matrices for each squeeze force and VT stimulus duration pairing, aggregated across all subjects. The probability of subjects correctly responding are given as a function of the stimulus site. Individual columns sum to 100%. The bottom left matrix combines all conditions. The total percentage of correct responses for each condition are given in the subplot titles. The bottom right inlay displays the approximate location of each stimulus relative to wrist and forearm anatomy, particularly the radial (R) and ulnar (U) bones. In general, we observe 1) identification rates are greatly reduced at stimulus sites located over bony areas, 2) subjects seem to perform better given a longer stimulus duration, and 3) the middle squeeze level of 5 N yields the best performance, suggesting that there may exist an optimum level of preload squeeze force.

performing pairwise comparisons between stimulus locations with a Bonferroni correction show that subjects perform significantly worse for the T1 and T5 stimuli locations ( $p < 0.005$  in all relevant comparisons). Unsurprisingly, feedback from subjects during the self-exploration phase suggested that these vibrotactors were most difficult to identify. The general consensus was that vibrotactors over bony areas of the wrist were more difficult to localize than those over soft tissue. Fig. 11(h) illustrates this

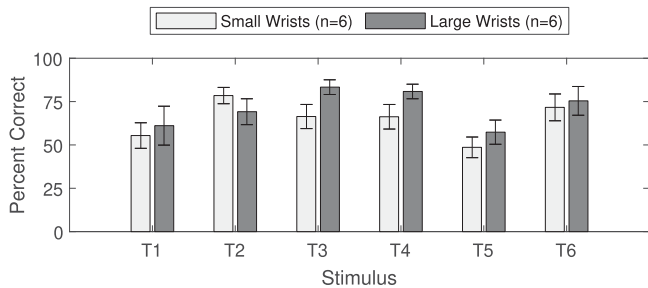


Fig. 12. Percentage of correctly identified vibrotactor stimuli for both groups of wrist size as a function of the stimulus location. The data represents the mean of all conditions, and error bars are for a 95% confidence interval.

phenomenon, where the approximate location the radial (R) and ulnar (U) bones can be seen.

Although the total percent correct in Fig. 11(e) and (f), along with qualitative feedback from subjects, suggests that identification rates decrease with higher levels of squeeze force, we find no significant difference for the main effect of squeeze force. While it seems probable that an effect could be found with a more nuanced study, it is reassuring to find that squeeze does not drastically interfere with the perception of vibration as experiments have shown for other combinations of multimodal cues (e.g., skin stretch and squeeze [24]).

The main effect of duration was also found to be significant, with the 250 ms stimulus providing more accurate responses [ $F(1,11)=5.63$ ,  $p = 0.037$ ]. This is evident when comparing the total percent correct between columns in Fig. 11. Interestingly, we note that the mean accuracy difference between the long and short stimuli increases as a function of squeeze force (1.6%, 2.5%, and 4.2% for 0.5, 5, and 10 N, respectively). However, this may only be a trend as we find no significant interaction between squeeze force and duration.

Finally, we note that subjects with large wrists ( $C \geq 185$  mm) perform significantly better than those with small wrists when analyzed across all conditions [ $t(430) = 2.97$ ,  $p = 0.003$ ]. Fig. 12 shows that the large wrist group outperforms the small wrist group at five of the six stimulus locations. This phenomenon was also observed in [36], and is not particularly surprising considering larger wrists spread adjacent factors further apart. This may also be a function of tissue impedance, as individuals with large wrists tend to exhibit higher concentrations of adipose tissue. A study that correlates identification accuracy with body mass index (BMI) would be an interesting follow-up.

### B. Study 2: Squeeze Difference Threshold

Our second study sought to characterize users' perception of wrist squeeze stimuli. Two common measures of haptic perceptual performance are the absolute and difference thresholds [68]. Here, we choose to focus on the latter, and attempt to quantify the just noticeable difference (JND) for wrist squeeze force. Although JND studies have been conducted for squeeze on the wrist and arm, they are typically quantified in units that are indirectly related to the perceived stimulus and are inherently

tied to the device with which the study was performed (e.g., the angular displacement of a motor used to produce squeeze [24], the linear displacement of a squeezing belt [64], or the axial load in a squeeze inducing shape memory alloy [57]). Because Tasbi has the ability to control directly for uniform squeeze force, we can quantify wrist squeeze in practical units of normal force against the skin. To our knowledge, this is the first reporting of such. Whether squeeze perception is linked to contact force, tissue displacement, or something else entirely remains an open question, but the results presented here should provide future designers and scientists with a more general understanding of wrist squeeze perception than what currently exists.

1) *Subjects and Procedures*: Study 2 involved the same subjects and procedures from Study 1 (see Section V-A1).

2) *Experiment Design*: To determine the squeeze threshold, the method of constant stimuli with a two interval forced choice (2IFC) procedure was used. On each trial, the subject was presented with two sequential squeezes cues and tasked with choosing the cue that squeezed harder, either the first or second. One cue was always the standard force level (7 N), and the other cue was one of 11 comparison levels (2–12 N in 1-N intervals). The standard was pseudo-randomly presented either first or second in a counterbalanced manner to mitigate the so-called *time error* of 2IFC procedures [68]. To eliminate reliance on temporal information, each squeeze cue was rate controlled to last 1 s regardless of the target force level, where Tasbi ramped up to the force level over 1/3 s, held the force for another 1/3 s, and then ramped down to no squeeze force over the remaining 1/3 s. A 1/4 s delay was placed between the first and second cues. Subjects made their selection in the GUI, and performed 550 trials, or 50 repetitions of each comparison level. The trials were evenly divided into five windows, separated by a 60-s break.

3) *Results*: Fig. 13 shows the proportion of times subjects indicated that each comparison squeeze level was greater than the standard level. The data was fit to a general linear model with a logit link function to estimate the psychometric function for each subject. The JND is defined as the difference between the 75% (or 25%) threshold and the 50% threshold [i.e., the point of subjective equality (PSE)]. Across all subjects, the JND for wrist squeeze force was found to be  $1.28 \pm 0.46$  N (mean + SD). Given the standard of 7 N, the Weber fraction was approximately 0.18. The PSE was  $7.10 \pm 0.24$  N, and corresponds well with the standard level.

The boxplot of JNDs for all subjects in Fig. 13(b) suggests that some subjects are far more perceptive to wrist squeeze than others, with JNDs ranging from as low as 0.72 N to as high as 2.07 N. In contrast to Study 1, we cannot attribute this difference to wrist size, which was found to have no significant effect on JND ( $t(10) = .48$ ,  $p = 0.65$ ). This further evidenced in Fig. 13(a) by comparing the mean psychometric functions of both the small and large wrist groups.

### C. Study 3: Maximum Comfortable Squeeze

In Study 3, we determined the maximum comfortable squeeze force and displacement using experimental psychophysics to inform the auction requirements for future wristband designs.

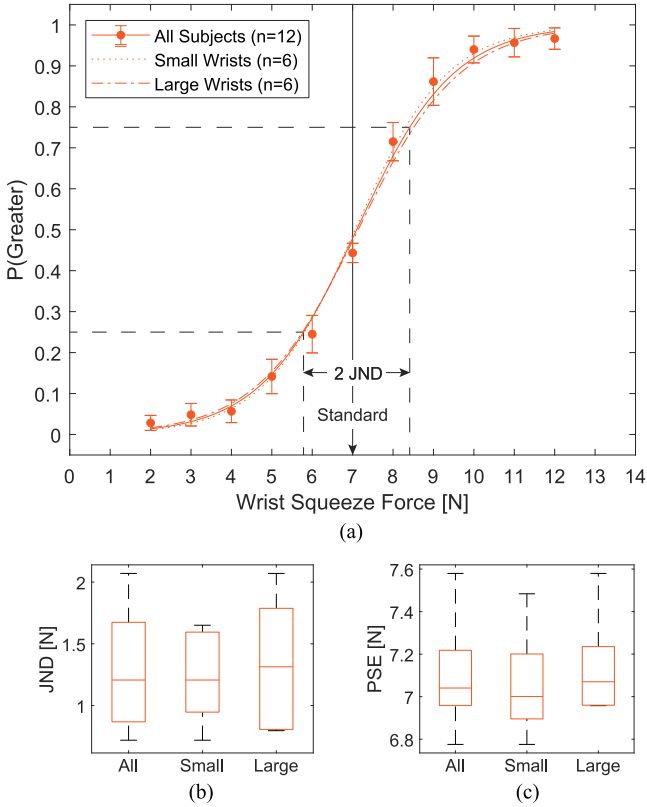


Fig. 13. (a) Mean psychometric function(s) experimentally determined for wrist squeeze force. Error bars represent a 95% confidence interval. (b) Mean difference threshold, or JND, was found to be 1.28 N. (c) PSE shows little bias from the standard of 7 N. Importantly, we find that wrist size has no significant effect on the JND.

Because Tasbi is equipped with force and position sensors, it is an ideal device to accurately determine the maximum comfort requirement for wrist squeeze. Here, we define squeeze force as the force measured internally by Tasbi’s capacitive sensor under the top-face housing, and displacement as the amount linear travel in Tasbi’s tensioning cord.

1) *Subjects and Procedures:* Study 3 involved a cohort of subjects recruited at Reality Labs Research. In accordance with IRB Protocol #IRB-20182617, six subjects (all male) participated in the experiment. All subjects were FRL employees, but were naive to the purpose of the experiment.

Subjects completed the task by interacting with an on-screen GUI using keyboard (left, right arrow key) input with their right hand. Tasbi was worn on the right wrist, and each subject’s arm was supported such that Tasbi was suspended over free space and not inadvertently resting on any surfaces. To prevent use of auditory cues, pink noise was played over headphones throughout the experiment.

2) *Experiment Design:* To determine the maximum comfortable squeeze force thresholds, the method of adjustment was used. On each trial, the device started at an initial squeeze level of approximately 3 N and subjects increased/decreased the squeeze force until it was perceptually at the upper limit of comfort. Subjects completed 10 repetitions to arrive at the maximum comfortable squeeze force threshold.

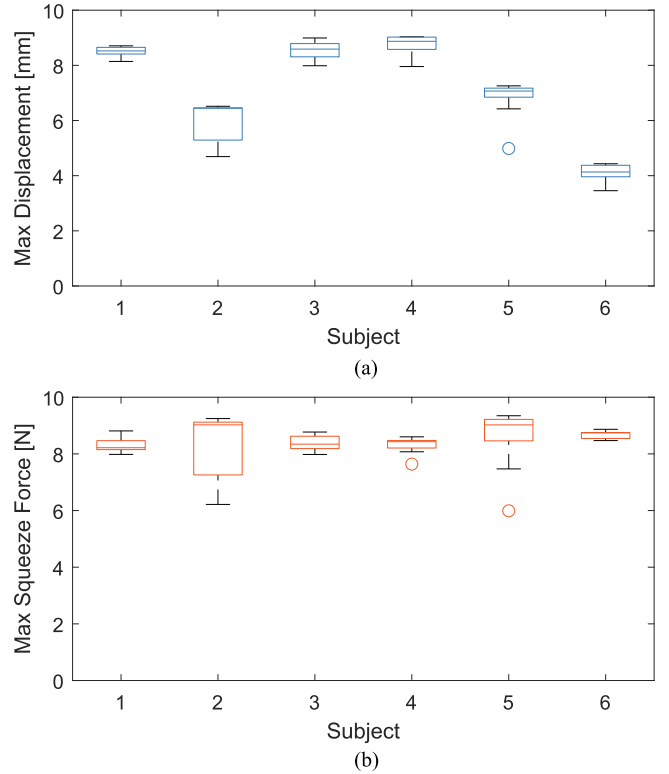


Fig. 14. Maximum comfortable squeeze in terms of (a) linear cord displacement and (b) rendered squeeze force. Though only six subjects are represented here, we note more consistency between subjects in terms of force rather than displacement. The mean max comfortable force was  $8.4 \pm 0.5$  N.

3) *Results:* The maximum comfortable force and displacement estimates are shown in Fig. 14(a) and (b), respectively. Results show that participants consistently chose a normal wrist squeeze force below  $F_N = 10$  N and displacement below 10 mm as the maximum comfortable wrist squeeze.

## VI. CONCLUSION

To conclude this article, we presented Tasbi, a haptic wrist-band featuring multimodal squeeze and vibration. Our design makes significant strides toward realizing a compact, all-day-wearable wrist interface, and, to our knowledge, is the smallest of its kind with an overall footprint of  $50 \times 30 \times 15$  mm and 120 g. We accomplished this through a novel tensioning mechanism that is both mechanically robust and squeeze efficient, producing peak normal forces up to 15 N without significant tangential losses. This mechanism allowed for a smaller motor selection which was important to both Tasbi’s overall size and potential to be battery powered in the future. The latter point is, of course, of long-term importance, and next steps will involve further miniaturizing the design and increasing transmission efficiency so that an onboard battery can be included. However, improvements to mechanical efficiency alone may ultimately be insufficient, so additional steps should be considered. For example, a distributed power system with multiple batteries located around the wrist could help in achieving an acceptable form factor. The application of novel battery technologies may

provide a path forward as well, as both printable [69] and multifunctional structural [70] batteries could allow for storing energy in the housing elements.

We further presented a responsive and accurate squeeze force control solution that makes use of a low-cost force sensing capacitor as well incremental encoder velocity estimation in a hybrid fashion. Across Tasbi's nominal force range of 0–10 N, the controller showed less than 5% tracking error, a 70-ms step response, and an overall bandwidth of 9.1 Hz. Unlike traditional methods of squeeze which leverage position control, force control offered the ability to provide consistent squeeze cues regardless of wrist impedance, size or posture.

Finally, with Tasbi's unique ability to control directly for squeeze force, we conducted two psychophysical studies of haptic perception ( $n = 12$ ). The first study tested subject's ability to identify stimuli from Tasbi's six vibrotactors under varying levels of static squeeze force, and offered the following insights: 1) Vibrotactor identification rates are affected by radial location, with vibrotactors over bony areas of the wrist being significantly more difficult to discern; 2) subjects with large wrists perform significantly better than those with small wrists; and 3) the amount of static squeeze has no significant effect on identification rates. The latter is a particularly important point for multimodal devices seeking to integrate squeeze and vibrotactile feedback. Our second study tested for the JND of wrist squeeze force, which we found to be 1.28 N averaged across all subjects. In contrast to vibration, we find that wrist size has no significant effect on this threshold. Our third study indicated that participants found wrist squeeze forces below 10 N to be comfortable.

Our main focal point moving forward is in applying Tasbi to real-world scenarios. Because of the device's versatility, almost any of the applications discussed in Section I could be studied with Tasbi. Our primary interest, however, is in exploring Tasbi's utility for AR/VR contexts. Already, we have found Tasbi to be highly capable in rendering immersive feedback for hand and finger interactions in VR [8]. Foreseeing AR as a transformative technology on the horizon, our future work will continue down this path and attempt to elucidate how individuals perceive referred haptic feedback from simple, wearable haptic devices.

## REFERENCES

- [1] K. J. Kuchenbecker, J. Fiene, and G. Niemeyer, "Improving contact realism through event-based haptic feedback," *IEEE Trans. Vis. Comput. Graph.*, vol. 12, no. 2, pp. 219–230, Mar./Apr. 2006.
- [2] V. Hayward *et al.*, "Haptic interfaces and devices," *Sensor Rev.*, vol. 24, pp. 16–29, Mar. 2004.
- [3] R. Sigrist *et al.*, "Augmented visual, auditory, haptic, and multimodal feedback in motor learning: A review," *Psychon. Bull. Rev.*, vol. 20, no. 1, pp. 21–53, 2013.
- [4] Y. Visell, "Tactile sensory substitution: Models for enactment in HCI," *Interacting Comput.*, vol. 21, no. 1–2, pp. 38–53, Aug. 2008.
- [5] F. Chinello, C. Pacchierotti, J. Bimbo, N. G. Tsagarakis, and D. Prattichizzo, "Design and evaluation of a wearable skin stretch device for haptic guidance," *IEEE Robot. Automat. Lett.*, vol. 3, no. 1, pp. 524–531, Jan. 2018.
- [6] C. Rossa, J. Fong, N. Usmani, R. Sloboda, and M. Tavakoli, "Multiactuator haptic feedback on the wrist for needle steering guidance in brachytherapy," *IEEE Robot. Automat. Lett.*, vol. 1, no. 2, pp. 852–859, Jul. 2016.
- [7] N. Dunkelberger *et al.*, "A multi-sensory approach to present phonemes as language through a wearable haptic device," *IEEE Trans. Haptics*, vol. 14, no. 1, pp. 188–199, Jan.–Mar. 2021.
- [8] E. Pezent *et al.*, "Explorations of wrist haptic feedback for AR/VR interactions with Tasbi," in *Proc. Extended Abstr. CHI Conf. Human Factors Comput. Syst.*, 2020, pp. 1–4.
- [9] N. Colella, M. Bianchi, G. Grioli, A. Bicchi, and M. G. Catalano, "A novel skin-stretch haptic device for intuitive control of robotic prostheses and avatars," *IEEE Robot. Automat. Lett.*, vol. 4, no. 2, pp. 1572–1579, Apr. 2019.
- [10] J. Mouchoux, S. Carisi, S. Dosen, D. Farina, A. F. Schilling, and M. Markovic, "Artificial perception and semiautonomous control in myoelectric hand prostheses increases performance and decreases effort," *IEEE Trans. Robot.*, vol. 37, no. 4, pp. 1298–1312, Aug. 2021.
- [11] J. F. Mullen, J. Mosier, S. Chakrabarti, A. Chen, T. White, and D. P. Losey, "Communicating inferred goals with passive augmented reality and active haptic feedback," *IEEE Robot. Automat. Lett.*, vol. 6, no. 4, pp. 8522–8529, Oct. 2021.
- [12] J. P. Clark *et al.*, "On the role of wearable haptics for force feedback in teleimpedance control for dual-arm robotic teleoperation," in *Proc. Int. Conf. Robot. Automat.*, 2019, pp. 5187–5193.
- [13] J. Wheeler, K. Bark, J. Savall, and M. Cutkosky, "Investigation of rotational skin stretch for proprioceptive feedback with application to myoelectric systems," *IEEE Trans. Neural Syst. Rehabil. Eng.*, vol. 18, no. 1, pp. 58–66, Feb. 2010.
- [14] K. J. Kim and D. Shin, "An acceptance model for smart watches: Implications for the adoption of future wearable technology," *Internet Res.: Electron. Netw. Appl. Policy*, vol. 25, pp. 527–541, Aug. 2015.
- [15] J. Choi and S. Kim, "Is the smartwatch an it product or a fashion product? A study on factors affecting the intention to use smartwatches," *Comput. Human Behav.*, vol. 63, pp. 777–786, 2016.
- [16] M. A. Baumann, K. E. MacLean, T. W. Hazelton, and A. McKay, "Emulating human attention-getting practices with wearable haptics," in *Proc. IEEE Hapt. Symp.*, 2010, pp. 149–156.
- [17] J. P. Clark, S. Y. Kim, and M. K. O'Malley, "The rice haptic rocker: Altering the perception of skin stretch through mapping and geometric design," in *Proc. IEEE Hapt. Symp.*, 2018, pp. 192–197.
- [18] S. Casini, M. Morvidoni, M. Bianchi, M. Catalano, G. Grioli, and A. Bicchi, "Design and realization of the CUFF-clenching upper-limb force feedback wearable device for distributed mechano-tactile stimulation of normal and tangential skin forces," in *Proc. IEEE Int. Conf. Intell. Robots Syst.*, 2015, pp. 1186–1193.
- [19] K. Bark, J. Wheeler, P. Shull, J. Savall, and M. Cutkosky, "Rotational skin stretch feedback: A wearable haptic display for motion," *IEEE Trans. Haptics*, vol. 3, no. 3, pp. 166–176, Jul.–Sep. 2010.
- [20] S. Song *et al.*, "Hot & tight: Exploring thermo and squeeze cues recognition on wrist wearables," in *Proc. Int. Symp. Wearable Comput.*, 2015, pp. 39–42.
- [21] P. Lopes *et al.*, "Providing haptics to walls & heavy objects in virtual reality by means of electrical muscle stimulation," in *Proc. ACM Conf. Human Factors Comput. Syst.*, 2017, pp. 1471–1482.
- [22] J. L. Sullivan *et al.*, "Multi-sensory stimuli improve distinguishability of cutaneous haptic cues," *IEEE Trans. Hapt.*, vol. 13, no. 2, pp. 286–297, Apr.–Jun. 2020.
- [23] D. Wang, K. Ohnishi, and W. Xu, "Multimodal haptic display for virtual reality: A survey," *IEEE Trans. Ind. Electron.*, vol. 67, no. 1, pp. 610–623, Jan. 2020.
- [24] Z. A. Zook, J. J. Fleck, T. W. Tjandra, and M. K. O'Malley, "Effect of interference on multi-sensory haptic perception of stretch and squeeze," in *Proc. IEEE World Hapt. Conf.*, 2019, pp. 371–376.
- [25] Y. Zheng and J. B. Morrell, "Haptic actuator design parameters that influence affect and attention," in *Proc. IEEE Hapt. Symp.*, 2012, pp. 463–470.
- [26] R. Wang *et al.*, "Keep in touch: Channel, expectation and experience," in *Proc. ACM Conf. Human Factors Comput. Syst.*, 2012, pp. 139–148.
- [27] D. Tsetserukou, "Haptihug: A novel haptic display for communication of hug over a distance," in *Haptics: Generating and Perceiving Tangible Sensations*, A. M. L. Kapperset *et al.*, Eds. Berlin, Heidelberg: Springer, 2010, pp. 340–347.
- [28] L. Meli, I. Hussain, M. Aurilio, M. Malvezzi, M. K. O'Malley, and D. Prattichizzo, "The hBracelet: A wearable haptic device for the distributed mechanotactile stimulation of the upper limb," *IEEE Robot. Automat. Lett.*, vol. 3, no. 3, pp. 2198–2205, Jul. 2018.
- [29] S. Biswas and Y. Visell, "Emerging material technologies for haptics," *Adv. Mater. Technol.*, vol. 4, no. 4, 2019, Art. no. 1900042.

- [30] E. Pezent *et al.*, "Tasbi: Multisensory squeeze and vibrotactile wrist haptics for augmented and virtual reality," in *Proc. IEEE World Hapt. Conf.*, 2019, pp. 1–6.
- [31] R. W. Cholewiak and A. A. Collins, "Vibrotactile localization on the arm: Effects of place, space, and age," *Perception Psychophys.*, vol. 65, no. 7, pp. 1058–1077, 2003.
- [32] I. Oakley *et al.*, "Determining the feasibility of forearm mounted vibrotactile displays," in *Proc. Symp. Hapt. Interfaces Virtual Environ. Teleoperator Syst.*, 2006, pp. 27–34.
- [33] H.-Y. Chen *et al.*, "Tactor localization at the wrist," in *Proc. EuroHapt.*, 2008, pp. 209–218.
- [34] S. Panéels *et al.*, "What's around me? multi-actuator haptic feedback on the wrist," in *Proc. World Hapt. Conf.*, 2013, pp. 407–412.
- [35] M. Matscheko *et al.*, "Tactor placement in wrist worn wearables," in *Proc. Int. Symp. Wearable Comput.*, 2010, pp. 1–8.
- [36] M. G. Carcedo *et al.*, "Hapticolor: Interpolating color information as haptic feedback to assist the colorblind," in *Proc. ACM Conf. Human Factors Comput. Syst.*, 2016, pp. 3572–3583.
- [37] A. Gupta *et al.*, "Direct manipulation in tactile displays," in *Proc. CHI Conf. Human Factors Comput. Syst.*, Ser. CHI '16, 2016, pp. 3683–3693.
- [38] F. Pece *et al.*, "Magtics: Flexible and thin form factor magnetic actuators for dynamic and wearable haptic feedback," in *Proc. 30th Annu. ACM Symp. User Interface Softw. Technol.*, Ser. UIST '17, 2017, pp. 143–154.
- [39] J. Hong *et al.*, "Evaluating angular accuracy of wrist-based haptic directional guidance for hand movement," in *Proc. Graph. Interface Conf. Can. Human-Comput. Commun. Soc.*, 2016, pp. 195–200.
- [40] M. Ogrinc, I. Farkhatdinov, R. Walker, and E. Burdet, "Sensory integration of apparent motion speed and vibration magnitude," *IEEE Trans. Hapt.*, vol. 11, no. 3, pp. 455–463, Jul.–Sep. 2018.
- [41] E. Pezent, B. Cambio, and M. K. O'Malley, "Syntacts: Open-source software and hardware for audio-controlled haptics," *IEEE Trans. Hapt.*, vol. 14, no. 1, pp. 225–233, Jan.–Mar. 2021.
- [42] S. C. Lee and T. Starner, *BuzzWear: Alert Perception in Wearable Tactile Displays on the Wrist*. New York, NY, USA: Association Computing Machinery, 2010, pp. 433–442.
- [43] S. J. Bolanowski *et al.*, "Four channels mediate the mechanical aspects of touch," *J. Acoust. Soc. Amer.*, vol. 845, pp. 1680–94, 1988.
- [44] S. J. Lederman and R. L. Klatzky, "Haptic perception: A tutorial," *Attention, Perception, Psychophys.*, vol. 71, no. 7, pp. 1439–1459, Oct. 2009.
- [45] H. Pohl *et al.*, "Squeezeback: Pneumatic compression for notifications," in *Proc. ACM Conf. Human Factors Comput. Syst.*, 2017, pp. 5318–5330.
- [46] D. Tsetseroukou *et al.*, "Affective haptics in emotional communication," in *Proc. Int. Conf. Affect. Comput. Intell. Interact. Workshops*, 2009, pp. 1–6.
- [47] T. Nakamura *et al.*, "Development of a wrist-twisting haptic display using the hanger reflex," in *Proc. 11th Conf. Adv. Comput. Entertainment Technol.*, 2014, pp. 1–5.
- [48] E. Treadway, B. Gillespie, D. Bolger, A. Blank, M. O'Malley, and A. Davis, "The role of auxiliary and referred haptic feedback in myoelectric control," in *Proc. IEEE World Hapt. Conf.*, 2015, pp. 13–18.
- [49] J. D. Brown, J. N. Fernandez, S. P. Cohen, and K. J. Kuchenbecker, "A wrist-squeezing force-feedback system for robotic surgery training," in *Proc. IEEE World Hapt. Conf.*, 2017, pp. 107–112.
- [50] A. A. Stanley and K. J. Kuchenbecker, "Evaluation of tactile feedback methods for wrist rotation guidance," *IEEE Trans. Haptics*, vol. 5, no. 3, pp. 240–251, Jul.–Sep. 2012.
- [51] R. Wang *et al.*, "Keep in touch: Channel, expectation and experience," in *Proc. SIGCHI Conf. Human Factors Comput. Syst.*, 2012, pp. 139–148.
- [52] M. Bianchi *et al.*, "Design and preliminary affective characterization of a novel fabric-based tactile display," in *Proc. IEEE Hapt. Symp.*, 2014, pp. 591–596.
- [53] J. J. Fleck, Z. A. Zook, T. W. Tjandra, and M. K. O'Malley, "A cutaneous haptic cue characterization testbed," in *Proc. IEEE World Hapt. Conf.*, 2019, pp. 319–324.
- [54] F. Chinello *et al.*, "The HapBand: A cutaneous device for remote tactile interaction," in *Haptics: Neuroscience, Devices, Model. Appl.*, M. Auvray and C. Duriez, Eds. Berlin, Heidelberg: Springer, 2014, pp. 284–291.
- [55] T. Moriyama *et al.*, "Development of a wearable haptic device that presents the haptic sensation corresponding to three fingers on the forearm," in *Proc. Symp. Spatial User Interaction*, 2018, pp. 158–162.
- [56] M. Sarac *et al.*, "Effects of haptic feedback on the wrist during virtual manipulation," in *Proc. IEEE Haptics Symp.*, [arxiv.org/abs/2204.05830](https://arxiv.org/abs/2204.05830).
- [57] A. Gupta *et al.*, "HapticClench: Investigating squeeze sensations using memory alloys," in *Proc. ACM Symp. User Interface Soft. Tech.*, 2017, pp. 109–117.
- [58] E. M. Young *et al.*, "Bellowband: A pneumatic wristband for delivering local pressure and vibration," in *Proc. IEEE World Hapt. Conf.*, 2019, pp. 55–60.
- [59] M. Zhu *et al.*, "Pneusleeve: In-fabric multimodal actuation and sensing in a soft, compact, and expressive haptic sleeve," in *Proc. CHI Conf. Human Factors Comput. Syst.*, 2020, pp. 1–12.
- [60] M. Raitor, J. M. Walker, A. M. Okamura, and H. Culbertson, "WRAP: Wearable, restricted-aperture pneumatics for haptic guidance," in *Proc. IEEE Int. Conf. Robot. Automat.*, 2017, pp. 427–432.
- [61] C. Payne *et al.*, "Force control of textile-based soft wearable robots for mechanotherapy," in *Proc. IEEE Int. Conf. Robot. Automat.*, 2018, pp. 5459–5465.
- [62] S. J. Kim, H. Chang, J. Park, and J. Kim, "Design of a portable pneumatic power source with high output pressure for wearable robotic applications," *IEEE Robot. Automat. Lett.*, vol. 3, no. 4, pp. 4351–4358, Oct. 2018.
- [63] M. Wehner *et al.*, "Pneumatic energy sources for autonomous and wearable soft robotics," *Soft Robot.*, vol. 1, no. 4, pp. 263–274, 2014.
- [64] M. Aggravi, F. Pausé, P. R. Giordano, and C. Pacchierotti, "Design and evaluation of a wearable haptic device for skin stretch, pressure, and vibrotactile stimuli," *IEEE Robot. Automat. Lett.*, vol. 3, no. 3, pp. 2166–2173, Jul. 2018.
- [65] C. Moussette, "Simple haptics: Sketching perspectives for the design of haptic interactions," Ph.D. dissertation, Umeå Univ., 2012.
- [66] M. Park *et al.*, "Recent advances in tactile sensing technology," *Micromachines*, vol. 9, no. 7, p. 321, 2018.
- [67] J. Sparks *et al.*, "Use of silicone materials to simulate tissue biomechanics as related to deep tissue injury," *Adv. Skin Wound Care*, vol. 28, pp. 59–68, Feb. 2015.
- [68] L. A. Jones and H. Z. Tan, "Application of psychophysical techniques to haptic research," *IEEE Trans. Hapt.*, vol. 6, no. 3, pp. 268–284, Jul.–Sep. 2013.
- [69] R. R. Kohlmeier *et al.*, "Composite batteries: A simple yet universal approach to 3D printable lithium-ion battery electrodes," *J. Mater. Chem. A*, vol. 4, no. 43, pp. 16856–16864, 2016.
- [70] L. E. Asp *et al.*, "Structural battery composites: A review," *Funct. Composites Struct.*, vol. 1, no. 4, 2019, Art. no. 042001.



**Evan Pezent** (Member, IEEE) received the B.S. degree from the University of Alabama, Tuscaloosa, AL, USA, in 2014, and the M.S. and Ph.D. degrees from Rice University, Houston, TX, USA, in 2017 and 2021, respectively, all in mechanical engineering.

Since 2018, he has been with Reality Labs Research, Redmond, WA, USA, developing haptic devices and interactions for augmented and virtual reality, where he has been a Research Scientist since 2021. During his studies in the Mechatronics and Haptic Interfaces Lab, Rice University, he worked on

a number of projects involving robotic exoskeletons and haptic devices. He has authored or coauthored papers in the fields of rehabilitation and training, wearable and vibrotactile haptic feedback, and multisensory integration.

Dr. Pezent was awarded the NSF IGERT Fellowship in 2017.



**Priyanshu Agarwal** (Member, IEEE) received the B.Tech. degree from the Motilal Nehru National Institute of Technology, Allahabad, India, in 2007, the M.S. degree from the State University of New York at Buffalo, Buffalo, NY, USA in 2012, and the Ph.D. degree from the University of Texas at Austin, Austin, TX, USA, in 2017, all in mechanical engineering.

Since 2017, he has been with Reality Labs Research, Meta, Redmond, WA, USA, where he is currently a Research Scientist, leading research on novel haptic interfaces for virtual and augmented reality

applications



**Jessica Hartcher-O'Brien** (Member, IEEE) received the B.Soc.S. degree in psychology and the M.A. degree in psycho-acoustics from Western Sydney University, Penrith, NSW, Australia, in 2003 and 2006, respectively, and the Ph.D. degree in experimental psychology - perception from the University of Oxford, Oxford, U.K., in 2012.

In 2017, she was a Faculty with the Perceptual Intelligence Labs, Delft University of Technology, where she established the PI-Touch Lab. Since 2020, she has been a Research Scientist with Reality Labs

Research, Meta, Redmond, WA, USA, and is currently exploring haptic encoding and multisensory processing mechanisms for virtual and augmented reality.

Dr. Hartcher-O'Brien was awarded a Fyssen Fellowship to explore perception-based objective measures for sensory substitution at the École Normale Supérieure, Paris, France, in 2013.



**Marcia K. O'Malley** (Fellow, IEEE) received the B.S. degree from Purdue University, West Lafayette, IN, USA, in 1996, and the M.S. and Ph.D. degrees from Vanderbilt University, Nashville, TN, USA, in 1999 and 2001, respectively, all in mechanical engineering.

She is currently the Thomas Michael Panos Family Professor in mechanical engineering, in computer science, and in electrical and computer engineering with Rice University, Houston, TX, USA, and directs the Mechatronics and Haptic Interfaces Laboratory.



**Nicholas Colonnese** (Member, IEEE) received the B.S. degree from the University of Washington, Seattle, WA, USA, in 2010, and the M.S. and Ph.D. degrees from Stanford University, Stanford, CA, USA, in 2012 and 2015, respectively, all in mechanical engineering.

Since 2016, he has been with Reality Labs Research, Meta, Redmond, WA, USA, and is currently a Research Science Manager, leading research on novel interfaces for augmented and virtual reality.